



**CHALMERS**  
UNIVERSITY OF TECHNOLOGY

## **Atom probe tomography investigation of 3D nanoscale compositional variations in CVD TiAlN nanolamella coatings**

Downloaded from: <https://research.chalmers.se>, 2024-04-19 11:51 UTC

Citation for the original published paper (version of record):

Qiu, R., Aboulfadl, H., Bäcke, O. et al (2021). Atom probe tomography investigation of 3D nanoscale compositional variations in CVD TiAlN nanolamella coatings. *Surface and Coatings Technology*, 426. <http://dx.doi.org/10.1016/j.surfcoat.2021.127741>

N.B. When citing this work, cite the original published paper.



# Atom probe tomography investigation of 3D nanoscale compositional variations in CVD TiAlN nanolamella coatings

Ren Qiu<sup>a,\*</sup>, Hisham Aboufadi<sup>a</sup>, Olof Bäcke<sup>a</sup>, Dirk Stiens<sup>b</sup>, Hans-Olof André<sup>a</sup>, Mats Halvarsson<sup>a</sup>

<sup>a</sup> Department of Physics, Chalmers University of Technology, SE-41296 Gothenburg, Sweden

<sup>b</sup> Walter AG, D-72072 Tübingen, Germany

## ARTICLE INFO

**Keywords:**  
CVD  
Coatings  
APT  
TEM  
TiAlN

## ABSTRACT

The cubic (Ti<sub>1-x</sub>Al<sub>x</sub>)N<sub>y</sub> (TiAlN) phase with a nanolamella structure, synthesized via low pressure chemical vapour deposition (LPCVD), has been widely used in wear-resistant coatings during the latest years. The nanolamella structured TiAlN coatings contain periodic and epitaxially grown Ti-rich [denoted as Ti(Al)N] and Al-rich [denoted as Al(Ti)N] lamellae. However, the chemical compositions of these nano-structures have not been fully revealed. In this study, the microstructure of the nanolamella TiAlN coating was studied using scanning and transmission electron microscopy (SEM and TEM), and the chemical content was investigated using atom probe tomography (APT) that provides three-dimensional composition data with good accuracy and a spatial resolution down to the nanometer scale. It was found that over- and under-stoichiometries of N exist for the Ti(Al)N and the Al(Ti)N lamellae, respectively. According to the previous simulation results, such over- and under-stoichiometries are due to metal (Al and Ti) and N vacancies, respectively. The Al(Ti)N lamellae have a chemical formula of (Ti<sub>0.12</sub>Al<sub>0.88</sub>)N<sub>0.90</sub>, and have 10% N vacancies. The Ti(Al)N lamellae have a chemical formula of (Ti<sub>0.70</sub>Al<sub>0.30</sub>)N<sub>0.97</sub>, and have 3% metal (Al and Ti) vacancies. In addition to the nanolamella structure, compositional variations on a scale of a few nm were found in both types of lamellae. In the Ti-richest volumes, the composition corresponds to (Ti<sub>0.72</sub>Al<sub>0.28</sub>)<sub>0.88</sub>N so a maximum of 12% of metal vacancies exists. In the Al-richest volumes, the composition corresponds to (Ti<sub>0.07</sub>Al<sub>0.93</sub>)N<sub>0.64</sub> so a maximum of 36% N vacancies exists. In addition, a small amount of Cl (around 0.1 at.%) was found in the coating, which could originate from the incomplete dissociation of chloride precursors during the CVD surface reaction.

## 1. Introduction

Nowadays most tools for metal cutting are made of cemented carbide substrates coated with thin wear-resistant coatings. This gives both high hardness and good toughness for withstanding the extreme mechanical and thermal loads generated during high-speed machining [1]. To obtain a good cutting performance, wear-resistant coatings must possess properties like high hot hardness, outstanding thermal and chemical stability, and good adhesion to the cemented carbide substrate [2]. (Ti<sub>1-x</sub>Al<sub>x</sub>)N<sub>y</sub> (TiAlN) is widely used as a hard coating for cutting tool applications [3–11]. The TiAlN phase is obtained via partly replacing Ti with Al atoms in the Ti face centered cubic (FCC) sublattice of TiN. With increasing Al content, TiAlN exhibits higher hot hardness and better oxidation resistance than TiN [6,7]. It is worth mentioning that the cubic TiAlN phase is metastable, and tends to decompose and form cubic TiN

and hexagonal AlN (h-AlN) phases at elevated temperatures, especially when the Al content is high. Typically, the TiAlN coatings are synthesized via physical vapour deposition (PVD) and chemical vapour deposition (CVD). The highest Al content reported for PVD TiAlN is  $x = 0.67$  [in (Ti<sub>1-x</sub>Al<sub>x</sub>)N<sub>y</sub>] [7,8]. During the last decade, TiAlN with high Al content ( $x > 0.8$ ) has been synthesized successfully by low pressure CVD (LPCVD) [6,11–13].

It has been shown in previous studies that the chemical composition of TiAlN influences its lattice parameter, electronic structure, and thermal and mechanical properties [14–17]. Changing the chemical composition of a TiAlN coating thus makes it possible to tune its properties accordingly, and thereby exploring possibilities to further develop the coating. Varying the chemical composition in PVD TiAlN is possible as adatoms incorporated in the deposited films are provided by the gas supply and sputtered metal species, and the Al/Ti ratio can be controlled

\* Corresponding author.

E-mail address: [renq@chalmers.se](mailto:renq@chalmers.se) (R. Qiu).

<https://doi.org/10.1016/j.surfcoat.2021.127741>

Received 14 September 2021; Accepted 16 September 2021

Available online 30 September 2021

0257-8972/© 2021 The Authors. Published by Elsevier B.V. This is an open access article under the CC BY license (<http://creativecommons.org/licenses/by/4.0/>).

by the fractions of metals sputtered [15]. Controlling N under- and over-stoichiometries has been achieved in PVD TiAlN through tuning the  $N_2$  gas flow with respect to the amount of metal species (Ti and Al) [15,18]. Since the CVD process is usually run at higher process temperatures where kinetic barriers for the formation of certain phases are easier overcome, CVD is more likely to yield equilibrium phases. In spite of this, methods have been developed to avoid the equilibrium phases and obtain cubic TiAlN coatings with high Al content [29]. These methods involve the formation of a nanolamella structure in the coating. In our previous work [6,12,19], we have demonstrated that TiAlN coatings with a nanolamella structure containing periodic Ti-rich [Ti(Al)N] and Al-rich [Al(Ti)N] nanolamellae may be formed using a rotational gas supply in the CVD process. Each gas rotation cycle was found to create one nanolamella period [12]. It was suggested that the temporal variation of the local gas environment, induced by the rotational gas supply, causes an oscillatory controlled surface reaction, which forms periodic nanolamellae with the different Al and Ti contents [12].

By comparing density functional theory (DFT) simulation results with the experimental data (including lattice parameters and elastic modulus) for PVD TiAlN coatings, Baben et al. found that N under-stoichiometry and over-stoichiometry are due to N vacancies and metal (Al and Ti) vacancies, respectively [20]. Euchner et al. argued that the formation energies of the N and metal vacancies are influenced by the Al to Ti ratio [21]. It is thus reasonable to assume that nanolamella structured TiAlN with iterating Al-rich [Al(Ti)N] and Ti-rich [Ti(Al)N] lamellae would exhibit periodic variation of N content at the nanometer scale.

In order to help understand the surface reaction kinetics correlated to the temporal gas environment during the CVD process, it is necessary to accurately evaluate the chemical composition of the TiAlN phase and its variation within the nanolamella structure. In addition, knowing the local chemical compositions helps to reveal physical properties of the material, such as electronic structure, lattice straining, thermal stability, hardness and elastic modulus. The Ti and Al contents in CVD nanolamella TiAlN have been studied previously by electron microscopy based energy-dispersive X-ray spectrometry (XEDS), and the composition of the Al(Ti)N lamellae was reported to be around  $(Ti_{0.1}Al_{0.9})N_y$  and that of Ti(Al)N exhibited more fluctuations but was typically  $(Ti_{0.5}Al_{0.5})N_y$  [6,12]. Paseuth et al. reported “semiquantitative” N contents measured using XEDS [y in  $(Ti_{1-x}Al_x)N_y$ ], and found (100) textured coatings to be under-stoichiometric with respect to N, and (111) textured coatings to be over-stoichiometric [22]. However, the accuracy of their results was limited due to the low energy resolution of XEDS (140–150 eV) and an overlap of the  $N K_{\alpha}$  (392 eV) peak with the Ti  $L_{\alpha}$  (452 eV) peak. Alternatively, Zalesak et al. measured N contents by electron energy loss spectroscopy (EELS) and found Al(Ti)N lamellae to be over-stoichiometric with respect to N, and Ti(Al)N to be under-stoichiometric [11]. However, cross sections of their EELS signals were not calibrated using samples with known chemical composition, and this influences the accuracy of EELS quantification. Therefore, the N contents in LPCVD TiAlN nanolamellae are still not fully known, and work remains to accurately quantify the chemical composition of CVD TiAlN nanolamella coatings.

Atom probe tomography (APT) enables examination of chemical concentrations in three dimensions (3D) at the nanoscale with a few part per million (ppm) chemical sensitivity, providing valuable insights about local compositions and segregation to interfaces [23]. In addition, 3D variations in nano-chemistry, hidden in the 2D projection of electron micrographs, are possible to reveal with APT data reconstruction. The Al, Ti and N concentrations in PVD  $(Ti_{1-x}Al_x)N_y$  coatings with various x and y values, both as-deposited and after annealing, have previously been analyzed using APT [15,18,24–30]. Generally, the N content was found to be higher in Ti-rich volumes than in Al-rich ones [25,26,28], and with a sufficiently high total nitrogen content an over-stoichiometry with respect to N was found in Ti-rich volumes [25,26]. In some cases, the mean chemical composition was also measured by Rutherford

backscattering (RBS) or elastic recoil detection analysis (ERDA) and was found to coincide well with APT data under optimized measuring conditions in some but not all cases [26,29,30]. Therefore, it would be very interesting to characterize CVD  $(Ti_{1-x}Al_x)N_y$  nanolamella coatings with high mean Al contents ( $x > 0.8$ ) using APT under optimized conditions in order to explore its microstructure, as well as to evaluate the distribution of N, making it possible to compare with TiAlN grown by PVD.

The aim of this study is to reveal the 3D variation on a nano-scale of chemical content, especially of N, in CVD TiAlN. A nanolamella structured TiAlN coating was synthesized via the LPCVD method using a rotational gas supply, and its microstructure was studied using scanning and transmission electron microscopy (SEM and TEM). Its nano-chemistry was then investigated in 3D using APT.

## 2. Materials and methods

### 2.1. CVD synthesis

A TiAlN coating was deposited on a cemented carbide (94 wt% WC and 6 wt% Co) substrate that had been pre-coated with a thin TiN layer, using a LPCVD process with a rotating gas supply of  $AlCl_3$ ,  $TiCl_4$ , and  $NH_3$  precursors. The microstructure of the same coating was also studied in our previous work [12]. More details of the CVD synthesis are given elsewhere [12,31].

### 2.2. Characterization methods

Thin foil lift-out specimens for TEM characterization, and tip specimen for APT analysis, were prepared using an FEI Versa 3D focused ion beam (FIB) — SEM instrument with an Omniprobe micromanipulator. The TEM lift-out was further polished using a concentrated, ultra-low energy Ar ion beam to make an ultra-thin sample [32]. TEM and scanning TEM (STEM) studies were carried out using an FEI Titan 80-300 TEM/STEM instrument equipped with a Schottky field emission gun (FEG) operated at 300 kV. A high angle annular dark field (HAADF) detector was used for Z-contrast imaging in the STEM mode.

Previous APT analyses have sometimes failed to produce quantitative results that agree with results obtained using ERDA [29,30] or RBS [26]. There are several reasons for this. One is the thermal tails present after the peaks in APT mass spectra, leading to peak overlaps [26], see Fig. 1. These tails are due to the limited thermal conductivity of TiAlN, leading to a slow cooling of the specimen tip after the fast heating by the laser pulse and therefore continued field evaporation for a short period of time after the pulse peak [33]. We have minimized this effect by using tips with a large shank angle (approximately  $14^\circ$  half cone angle) to maximize cooling, and by using modest pulse power to limit the amount of heat to be conducted away [34]. It is also important to have mass limits for the peaks that encompass the whole tail; failure to do so might result in erroneous results [29,30].

Another reason for problems with quantitative analyses, in particular of carbides and nitrides, is the dead-time of the detector [35]. This effect is most serious for atomic species with one dominating isotope, such as N (99.6%) and Al (100%) but also Ti (74%). Nitrogen has propensity to field evaporate together with other nitrogen atoms and together with metal atoms. These molecular ions might survive the short acceleration time and appear in the mass spectrum as molecular ions, as evidenced by the peaks  $N_2^+$ ,  $AlN^{2+}$  and  $TiN^{2+}$  in Fig. 1. However, more highly ionised molecular species might also form but dissociate before acceleration and thus appear as two atomic ions in the spectrum, e.g.  $N_2^{2+}$  might dissociate to two  $N^+$ . If these ions happen to have the same mass, i.e. be of the same isotope, there is a high risk that these two ions striking the ion detector (an array of multichannel plates) at essentially the same time and at the same position will be registered as only one ion. A simple check for the occurrence of dead-time effects is to examine the isotope distribution of N and Ti. It is evident that the dead-time effect must have affected the recent data by Hans and Schneider, since in their data the

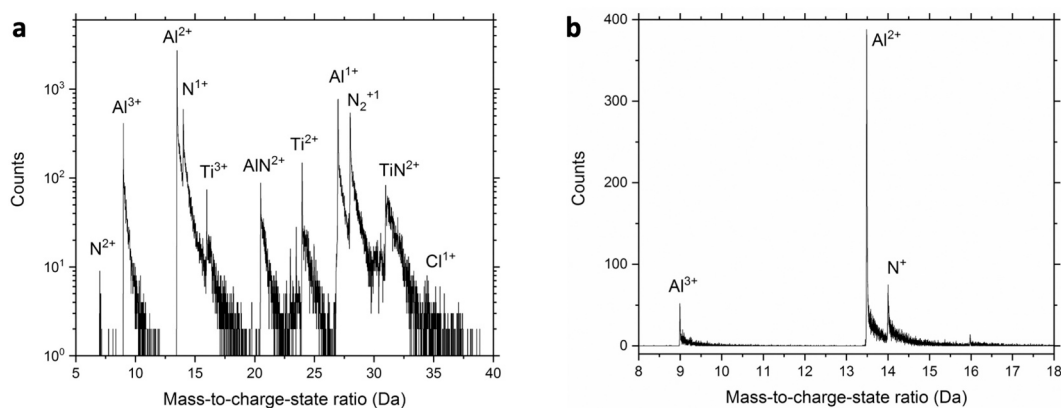


**Fig. 1.** APT data. (a) Full mass spectrum of the data used in the APT reconstruction presented in Fig. 3, where counts (number of atoms) are shown in logarithmic scale. (b) Mass spectrum from 8 to 18 Da highlighting  $\text{Al}^{3+}$ ,  $\text{Al}^{2+}$ , and  $\text{N}^+$  peaks. Very little of the  $\text{Al}^{2+}$  peak (estimated to be in the range of 0.1 at.%) overlaps the  $\text{N}^+$  peak.

minor isotopes have a much higher occurrence than the natural isotope abundance [29,30].

A third possibility for quantitative errors in APT analysis of nitrides is the formation of a neutral  $\text{N}_2$  molecule (and an  $\text{N}^+$  ion) upon dissociation of  $\text{MN}_3^{2+}$  ions, as suggested by Gault et al. for APT analysis of GaN [32]. This dissociation is expected to appear at a much lower electric field that occurring in our analyses (electric field estimated here to be 39–40 V/nm), and  $\text{MN}_3^{2+}$  ions are then also expected to appear in the spectrum. Since we never observed any nitride ions with more than one N atom, this effect cannot possibly be operating during our analysis.

Our APT measurements were performed in an IMAGO LEAP 3000× HR instrument, with a specimen base temperature of  $\sim 60$  K and a laser pulse energy set to 0.5 nJ. A pulse repetition rate of 200 kHz and a target evaporation rate of 0.2% were applied. These conditions gave the expected isotope distributions and a minimum of signal overlaps at thermal tails. The IVAS 3.6.10 software (CAMECA) was used for the data reconstruction and evaluation.

### 3. Results

#### 3.1. Textured growth and nanolamella microstructures

The deposited TiAlN coating has earlier been found to exhibit a

strong 111 texture [12]. As a result, the highly textured grains exhibit a pyramidal surface morphology, as seen in the SEM micrograph shown in Fig. 2(a). On the surface of the grains, there are three {001} facets, displaying a three-fold rotational symmetry along the [111] axis. The geometrical relationship between the growth facets and the internal nanolamella structure is illustrated by the STEM HAADF micrograph shown in Fig. 2(b). The HAADF Z-contrast reflects the local distribution of elements, where brighter and darker contrast corresponds to Ti(Al)N and Al(Ti)N lamellae, respectively.

As illustrated in Fig. 2(b), the Ti(Al)N and Al(Ti)N nanolamellae grow epitaxially along the  $\langle 001 \rangle$  directions, and the nanolamella interfaces are {001}. The formation of the {001} facets are probably sustained by the lower surface energy of {001}, according to DFT simulations performed by Forslund et al. [36].

#### 3.2. APT reconstructions and comparison with TEM analysis

Fig. 1 shows the APT spectrum of the LPCVD TiAlN specimen analyzed. It is worth noting that no clear peak of O is seen in the mass spectrum, therefore no oxidation of the coating is expected to have happened. Small  $\text{Cl}^{1+}$  peaks are identified at 35.0 and 37.0 Da, which indicate the existence of small amounts of Cl (approximately 0.1 at.%), possibly stemming from incomplete dissociation of chloride precursors

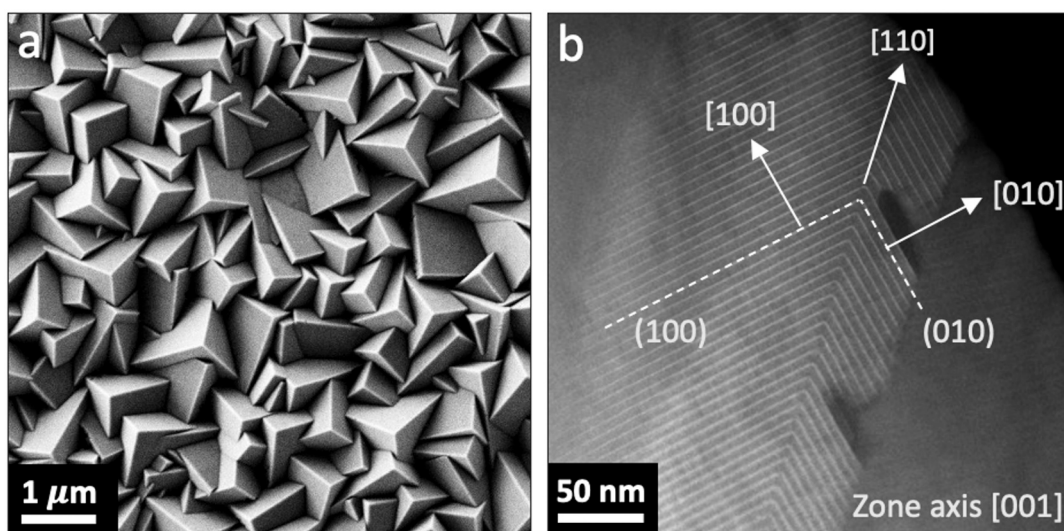


**Fig. 2.** CVD TiAlN grains with a pyramidal surface morphology and nanolamella internal structure. (a) SEM secondary electron (SE) micrograph of the coating surface. (b) STEM HAADF micrograph of the coating cross section.

during the surface reaction, although the content of Cl is very small compared to the other elements (Al, Ti and N).

In Fig. 3, APT reconstructions of the LPCVD TiAlN sample are shown, where a periodic nanolamella structure containing Ti(Al)N and Al(Ti)N lamellae can be clearly recognized. A tomographic slice (with thickness of around 2.4 nm) of the reconstruction is presented here showing atom maps with overlaid isoconcentration surfaces, see Fig. 3(a–c). Isoconcentration surfaces of Ti, Al and N are used in order to highlight the distribution of Ti-rich and Al-rich, as well as N-rich, volumes in the specimen. Large variations in the distribution for all three elements can be seen in these ATP reconstructions and neither the Ti(Al)N nor the Al(Ti)N nanolamellae show a homogenous distribution of Al and Ti. Instead, both the Ti(Al)N and Al(Ti)N nanolamellae consist of nanodomains richer and poorer in Ti (poorer and richer in Al, correspondingly). The Ti(Al)N nanolamellae show larger compositional fluctuations in comparison to the Al(Ti)N nanolamellae. The domains also appear to have an interconnected and entangled 3D network across the nanolamellae (see supplementary material for 360° view of the dataset). Concentration maps for each of the elements have been calculated from slices in the 3D volume and are also presented, see Fig. 3 (d–f), where the compositional fluctuations in the Ti(Al)N and Al(Ti)N are better visualized.

The isoconcentration surfaces and the concentration maps for N show that the N concentration fluctuates along with the Ti and the Al concentrations (Fig. 3). A higher N content is found in the Ti(Al)N lamellae, especially in regions with higher Ti content. It is important to note that accurate quantification of N concentrations using APT in

binary or ternary nitrides has been shown to be highly dependent on measuring parameters in APT [37,29], which stems from preferential evaporation effects and/or high multiple ion detector hits specific for measurements of such materials, which results in lower chemical quantification accuracy [38,39]. However, in this work we have used optimal measuring parameters that have been shown in other APT studies on TiAlN or TiN using similar APT instrumentation to display close agreement to the expected N content, evaluated by time-of-flight (TOF)-ERDA [15,40].

The distribution of the elements in 3D reveals features (see supplementary material for 360° view of the dataset) that are not visible in 2D projections of the nanolamella structure, e.g., electron micrographs obtained by STEM on samples with a standard thickness (around 100 nm). Instead of having uniform compositions and sharp interfaces, the TiAlN nanolamellae were found to exhibit chemical content fluctuations on a nano-scale, leading to lamellae of varying thickness. Fig. 4(a) shows a high-resolution STEM (HRSTEM) HAADF micrograph collected from a lift-out sample with a thickness (along the TEM imaging (out of paper) direction) of around 100 nm. According to the Z-contrast of Fig. 4(a), a slight variation of the Ti/Al ratio can be identified in both the Ti(Al)N and Al(Ti)N nanolamellae. The lift-out sample was further polished to obtain a thickness closer to the length scale for the fluctuations in Ti/Al ratio seen in the ATP reconstructions. Fig. 4(b) shows an inhomogeneity of chemical content revealed in an ultra-thin sample with a thickness (along the TEM imaging (out of paper) direction) less than 10 nm. It is found, according to the STEM HAADF imaging of the ultra-thin sample, that the nanolamellae, especially the Ti(Al)N lamellae, are composed of

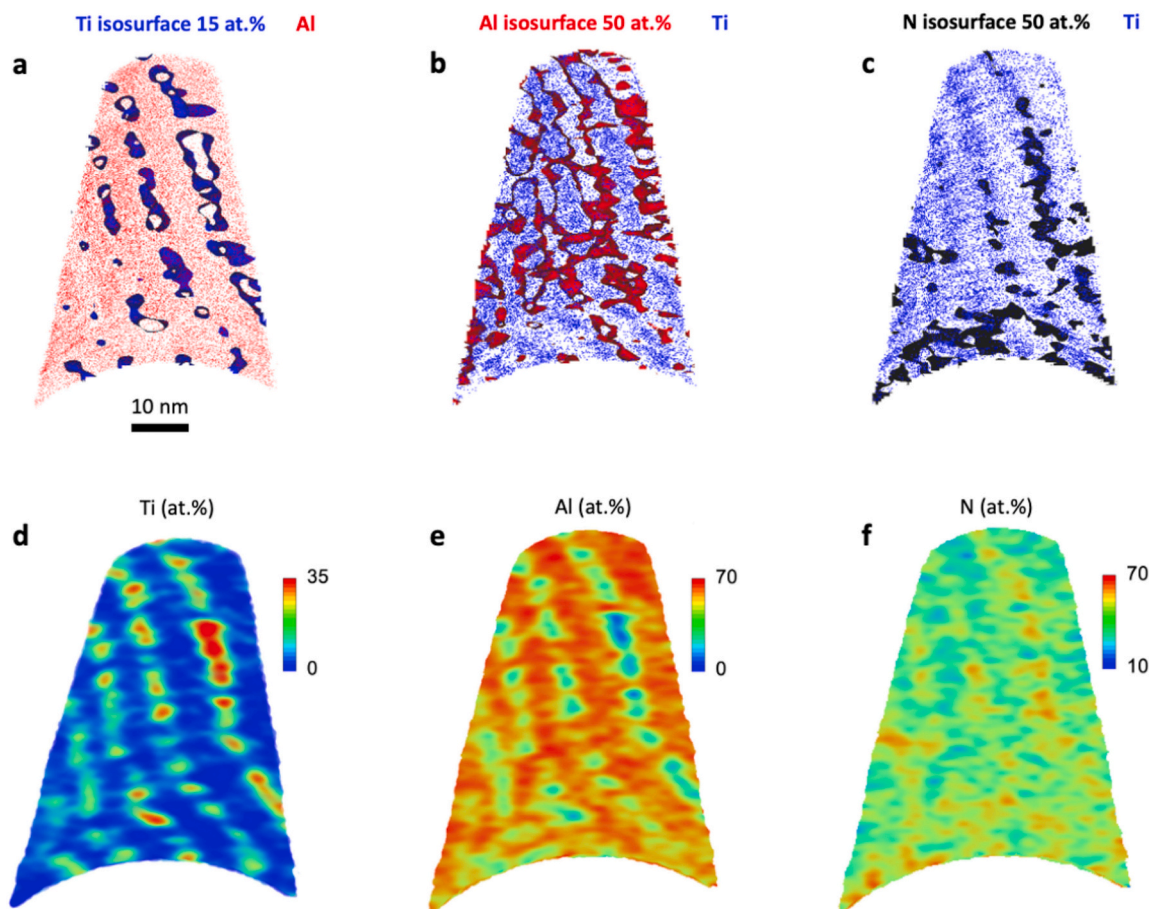


**Fig. 3.** APT analysis of the nanolamella structured TiAlN, showing 2.4 nm tomographic slices in the 3D reconstruction. In each reconstruction the elemental distribution of different elements is highlighted. (a) Al atoms shown in red color overlaid with isoconcentration surfaces of Ti (blue) of 15 at.%. (b) Ti atoms shown in blue color overlaid with isoconcentration surfaces of Al (red) of 50 at.%. (c) Ti atoms shown in blue color overlaid with isoconcentration surfaces of N (black) of 50 at.%. (d–f) 2D concentration maps for Ti, Al and N.

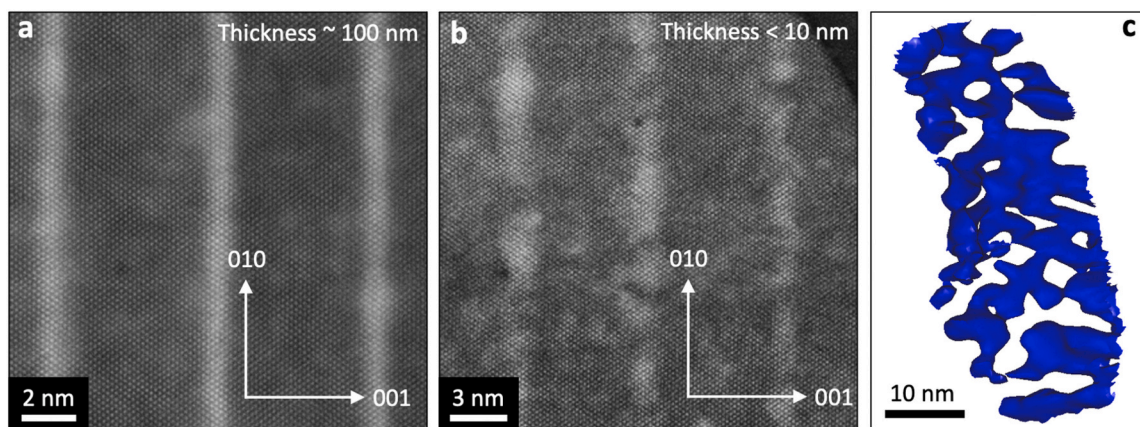


**Fig. 4.** 2D projection (sample thickness) effect of compositional inhomogeneity within the TiAlN nanolamellae. HRSTEM HAADF micrographs of samples with a thickness of (a) around 100 nm and (b) less than 10 nm. (c) APT isosurface for a Ti content of 15 at.% for a single TiAlN nanolamella.

domains with local high Ti/Al ratio (bright lamellae). However, in the thicker sample (Fig. 4(a)), this content fluctuation is hidden due to the 2D projection effect in TEM imaging. Fig. 4(c) is an APT 3D isosurface reconstruction of 15 at.% Ti content, which shows the fluctuating distribution of the chemical content in 3D.

### 3.3. Chemical composition of nanolamellae

The variation of the Ti, Al and N content in the TiAlN coating is further investigated by analyzing the APT data within a cylinder of 10 nm diameter positioned along the normal direction of the periodic nanolamellae, as indicated in Fig. 5. Fig. 5(a) and (b) show Al atoms in the reconstructions overlaid with isoconcentration surfaces of Ti, where Fig. 5(b) is rotated by 90° with respect to Fig. 5(a) to display the nanolamellae and the position of the cylinder. The 1D concentration profiles are presented in Fig. 5(c) showing the variation of Ti, Al and N

contents across the nanolamellae. In the Al(Ti)N lamellae, the Ti, Al, and N average content estimated from the profiles is 6.3 at.%, 46.3 at.%, and 47.4 at.%, respectively. The corresponding chemical formula is thus  $(\text{Ti}_{0.12}\text{Al}_{0.88})\text{N}_{0.90}$  (summarized in Table 1). The under-stoichiometry of N is represented as N vacancies in the chemical formula, according to the argument of Baben et al. that forming metal interstitials is less energetically favourable compared to forming N vacancies for the cubic TiAlN phase with N under-stoichiometry [20]. The average chemical composition of the Al(Ti)N lamellae thus implies 10% N vacancies compared to the metal sites (Al and Ti). The Al/Ti ratio is close to 90/10, which agrees with the XEDS results reported by Qiu et al. and Paseuth et al. [6,12,22]. In the Ti(Al)N lamellae, the Ti, Al, and N average content estimated from the profiles is 14.4 at.%, 34.8 at.%, and 50.7 at.%, respectively. The corresponding chemical formula is thus  $(\text{Ti}_{0.30}\text{Al}_{0.70})_{0.97}\text{N}$  (summarized in Table 1). The over-stoichiometry of N is represented by vacancies on metal sites (Ti and Al) in the chemical

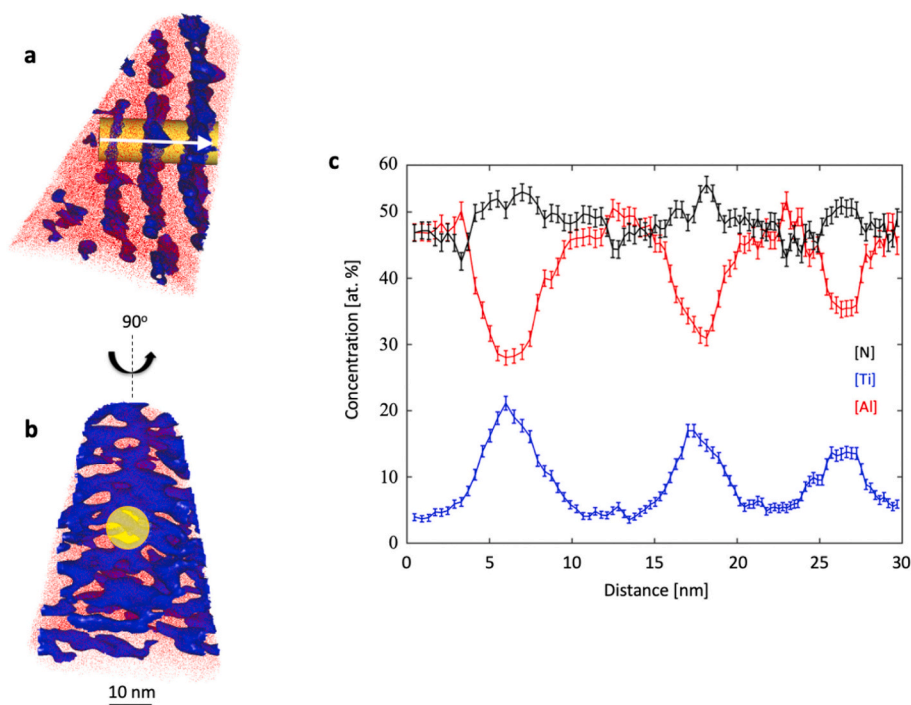


**Fig. 5.** (a) 3D reconstruction with Al atoms (red dots) and overlaid isoconcentration surfaces of Ti (15 at.%) shown in different orientations. (b) Sample rotated 90°. A cylinder is shown in the reconstructions from which the 1D profile is calculated. (c) 1D concentration profiles of Ti, Al and N in the cylinder along the direction marked by the arrow in (a).

**Table 1**

Summary of chemical compositions of the average for the TiAlN coating, the Al-rich lamellae [Al(Ti)N], the Ti-rich lamellae [Ti(Al)N], the Al-richest volume, the Ti-richest volume, and the volume with chemical stoichiometry. Elements given in atomic percent (at.%). The under- and over-stoichiometries of N are considered as vacancies in the N and metal sublattices, respectively, as proposed by Baben et al. [20].

	Al	Ti	N	Formula
Average	42.6	8.9	48.5	(Ti <sub>0.17</sub> Al <sub>0.83</sub> )N <sub>0.94</sub>
Al(Ti)N	46.3	6.3	47.4	(Ti <sub>0.12</sub> Al <sub>0.88</sub> )N <sub>0.90</sub>
Ti(Al)N	34.8	14.4	50.7	(Ti <sub>0.30</sub> Al <sub>0.70</sub> )N <sub>0.97</sub>
Al-richest	57.0	4.0	39.0	(Ti <sub>0.07</sub> Al <sub>0.93</sub> )N <sub>0.64</sub>
Ti-richest	13.0	34.0	53.0	(Ti <sub>0.72</sub> Al <sub>0.28</sub> )N <sub>0.88</sub>
Stoichiometric	40.8	9.2	50.0	(Ti <sub>0.18</sub> Al <sub>0.82</sub> )N

formula, according to the argument of Baben et al. that forming N interstitials is less energetically favourable compared to forming metal vacancies [20]. The average chemical composition of the Ti(Al)N lamellae thus implies 3 at% metal vacancies. The Al/Ti ratio is 30/70, which differs from the XEDS results reported previously (43/57 [12], 50/50 [6], and 38/62 [13]). In addition, the mean composition of TiAlN (averaging over multiple nanolamellae) is Al 42.6 at.%, Ti 8.9 at.%, and N 48.5 at.%, giving the chemical formula (Ti<sub>0.17</sub>Al<sub>0.83</sub>)N<sub>0.94</sub> (summarized in Table 1).

### 3.4. Depth profiling by proxigram

Due to the complex and entangled structure of the Ti richer and poorer (Al poorer and richer) regions in the Ti(Al)N lamellae and the rough interfacial morphology, measuring a composition profile across the nanolamellae calculated within a cylinder volume is not ideal to accurately evaluate the fluctuating compositions observed within the 3D reconstructions. Artefacts are introduced in the profile measurements; i. e. artificial intermixing across the interfaces, since it is not possible have a given analysis direction simultaneously perpendicular to all lamella interfaces. Furthermore, due to the limited detection efficiency of the APT technique (~37%) analyzing very small volumes within the dataset (e.g. the 10 nm diameter cylinder region) increases the statistical error in the profile analysis (low ion counts) [41]. Proximity histogram (proxigram) calculates 1D profiles across an isoconcentration surface of a given chemical composition, which to a large extent is independent of the interfacial morphology [41]. Moreover, larger volumes are possible

to analyze in the dataset, which provides lower statistical error and improves the accuracy of the profile calculation.

Fig. 6(a) and (b) shows two proxigram profiles calculated across isoconcentration surfaces with chemical compositions of 50 at.% Al and 15 at.% Ti. Fig. 6(a) shows that the Al content increases (and the Ti content correspondingly decreases) towards the centre of the Al(Ti)N lamellae (marked by red background). Fig. 6(b) shows that the Ti content increases (the Al content decreases) towards the centre of the Ti(Al)N lamellae (blue background). The elemental concentrations inside the Al(Ti)N and Ti(Al)N lamellae are of interest to investigate further. In the Al(Ti)N nanolamellae, the Al content reaches a maximum (plateau marked by a dotted line in Fig. 6(a)) of around 57 at.%, with approximately 4 at.% Ti and 39 at.% N (summarized in Table 1). In the Ti-rich parts of the Ti(Al)N lamellae, the Ti content reaches a maximum (dotted line in Fig. 6(b)) of around 34 at.%, with approximately 13 at.% Al and 53 at.% N (summarized in Table 1). It is apparent that the N content increases with a higher Ti content (lower Al content).

A variation of the chemical non-stoichiometry upon varying Ti and Al contents is also revealed, as the full chemical formulas for the Ti-richest (in the Ti(Al)N lamellae) and the Al-richest (in the Al(Ti)N lamellae) regions are (Ti<sub>0.72</sub>Al<sub>0.28</sub>)N<sub>0.88</sub> and (Ti<sub>0.07</sub>Al<sub>0.93</sub>)N<sub>0.64</sub>, respectively (summarized in Table 1). In the Ti richest regions an over-stoichiometry of N exists with 12% vacancies on the metal sites (Al and Ti), while in the Al richest regions, there is an under-stoichiometry of N corresponding to 36% N vacancies. The region with N stoichiometry is marked by a gray background in Fig. 6(a), where the Al, Ti and N contents are 40.8 at.%, 9.2 at.%, and 50 at.%, respectively, and thus the chemical formula is (Ti<sub>0.18</sub>Al<sub>0.82</sub>)N (summarized in Table 1).

In addition, it is worth mentioning that traces of Cl in the coating were detected with APT (see Fig. 1), which implies incomplete dissociation of chloride precursors during the surface reaction in CVD, although the Cl content is very low (around 0.1 at.%) and is found to be homogenous in the coating.

## 4. Discussion

### 4.1. 3D variation of chemical content in CVD nanolamella TiAlN

As shown in the results section, the 3D variation of the chemical content in the CVD nanolamella TiAlN phase includes two parts: the varying composition correlated with the periodic nanolamella structure (in the present case with a periodicity of around 10 nm, Fig. 5(c)) and

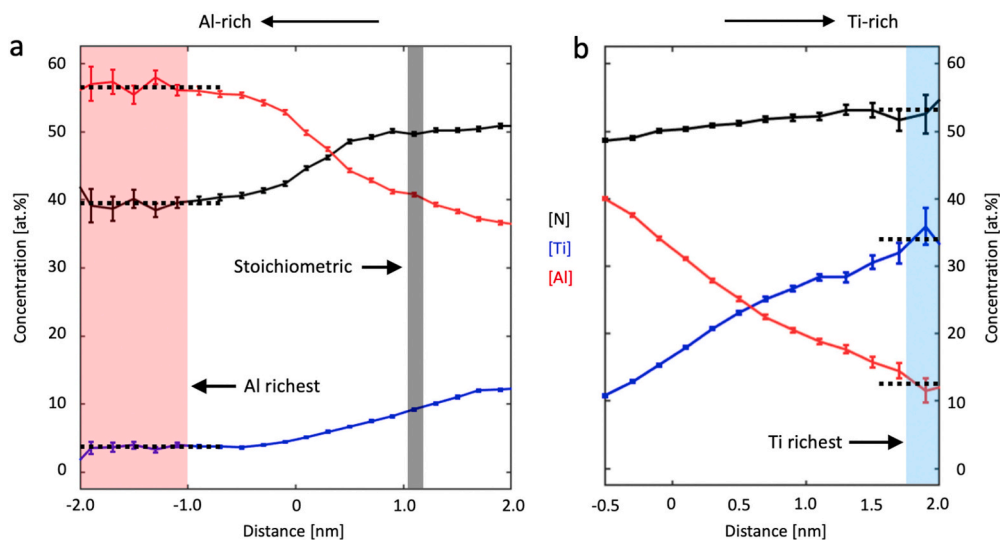


**Fig. 6.** (a) Proxigrams across isoconcentration surfaces with compositions of 50 at.% Al. (b) Proxigram analysis across isoconcentration surfaces with compositions of 15 at.% Ti. Regions with the highest Al and Ti contents are marked with red and blue background in (a) and (b), respectively. The chemical compositions of these regions are approximated by the heights of plateaus marked by dotted lines. The stoichiometric composition is marked with gray background in (a).

the local chemical fluctuation within the nanolamellae on a nanometer scale (Figs. 3 and 4).

According to the APT results (Table 1), the mean chemical content is found to be  $(\text{Ti}_{0.17}\text{Al}_{0.83})\text{N}_{0.94}$ , which is close to the stoichiometric content  $(\text{Ti}_{0.18}\text{Al}_{0.82})\text{N}$ , but with a slight N under-stoichiometry. The Al (Ti)N lamellae have a chemical formula of  $(\text{Ti}_{0.12}\text{Al}_{0.88})\text{N}_{0.90}$ , and thus contain 10% N vacancies on average. The Ti(Al)N lamellae have a chemical formula of  $(\text{Ti}_{0.30}\text{Al}_{0.70})_{0.97}\text{N}$ , and contain 3% metal (Al and Ti) vacancies on average. The Al/Ti ratio of the bulk TiAlN obtained by APT is close to that obtained by XEDS in analytical electron microscopy, considering its limitation of determining chemical content due to electron beam broadening in thin foil specimens and the 2D projection effect [6,12].

According to the proxigrams shown in Fig. 6, the maximum N vacancies reach 36% for the Al-richest regions ( $x = 0.93$ ), and the Ti(Al)N lamellae contain metal vacancies, reaching a maximum of 12% for the Ti-richest regions ( $x = 0.28$ ). This means that there are areas in the Al (Ti)N and the Ti(Al)N nanolamellae that have extreme N non-stoichiometries, although the corresponding volumes in the coating might be small. In addition, these areas have highest or lowest Al and Ti contents (the Al-richest and Ti-richest volume as indicated in Fig. 6) and correspond to the observed compositional variations on a nano-scale within the nanolamellae (see Fig. 4).

The periodic variation of chemical content of the TiAlN on a nanometer scale could cause different thermal and mechanical properties for the coating. Schramm et al. argued that more N vacancies reduce the mixing energy and thus increase the thermal stability of PVD TiAlN against spinodal decomposition [15]. In our nanolamella structured LPCVD TiAlN coating, the Al(Ti)N lamellae contain significant amount of N vacancies (up to 36%), suggesting a promoted thermal stability. In addition, it indicates that obtaining the high Al content [ $x > 0.9$  in  $(\text{Ti}_{1-x}\text{Al}_x)\text{N}_y$ ] in CVD TiAlN could be partly because of the high content of N vacancies induced during the CVD process. The observed variations in chemistry on a nano-scale will also affect the local lattice parameters and induce considerable strain fields. The elastic properties should also change with chemistry. Both the variations in strain and in elastic properties will increase the interaction with dislocations, making dislocation movement more difficult and therefore increasing the hardness. More N vacancies have been reported to increase the hardness of TiN, due to a higher rate-limiting activation energy for cation migration and an associated decrease of dislocation mobility [14,16]. The Al(Ti)N lamellae in CVD TiAlN coating thus could exhibit higher hardness due to more N vacancies, and the Ti(Al)N lamellae lower hardness due to N excess. This would lead to a periodic variation of hardness on the nanometer scale in the nanolamella structure. In addition, more N vacancies in TiAlN was reported to lower the elastic modulus [14], and higher Al content was reported to decrease the elastic modulus of TiAlN [17]. Correspondingly, using our results, the Al(Ti)N lamellae that are associated with a high Al content and N vacancy content would have a lower elastic modulus, compared to the Ti(Al)N lamellae, and the nanolamella structure would exhibit a periodic variation of elastic modulus on a nanometer scale.

#### 4.2. N non-stoichiometry and Al/Ti ratio

In this section, the N non-stoichiometry correlated to the variation of the Al/Ti ratio is discussed. Euchner et al. performed DFT simulations on the TiAlN system and found that relatively lower formation energies of metal (Ti and Al) than N vacancies exist for a wide range of compositions [ $0.3 < x < 0.9$  in  $(\text{Ti}_{1-x}\text{Al}_x)\text{N}_y$ ] ( $0 < y < \pm 0.0625$ ) [21]. A minimum formation energy for metal vacancies was found at  $x = 0.6$  [in  $(\text{Ti}_{1-x}\text{Al}_x)\text{N}_y$ ], which coincides with the APT results of this study, where metal vacancies (and the corresponding N over-stoichiometry) are found in Ti-rich [Ti(Al)N] volumes [ $x \sim 0.7$  in  $(\text{Ti}_{1-x}\text{Al}_x)\text{N}_y$ , see Table 1]. However, for  $x > 0.9$ , the formation energies are lower for N vacancies than for metal vacancies, according to the DFT simulations [21]. This could

explain the N vacancies (and the corresponding N under-stoichiometry) observed in the Al-rich volumes by APT in this study. It is worth noting that their (standard) DFT simulations is performed at a temperature of 0 K, and thus does not include contribution of lattice phonons for the total energy. The CVD process is performed at a relatively high temperature (923–1023 K) which probably influences the formation of N and/or metal vacancies significantly. In addition, the formation of N and metal vacancies in the TiAlN are also influenced by the kinetics of the CVD reaction and the formation of other types of defects (such as dislocations). However, these are not considered in the DFT simulations.

Similar to the results of this study, Rachbauer et al. reported a local non-stoichiometry in annealed (at 950 and 1350 °C) PVD TiAlN coatings that had been deposited close to stoichiometry [25,26]. Rachbauer et al. showed using APT proxigram analysis that slight over- and under-stoichiometries of N appears in the Ti- and Al-rich regions, respectively, which was caused by spinodal decomposition during annealing [25]. This suggests a diffusion of N atoms from the Al rich domains to the Ti rich domains, coupled to the diffusion of Al and Ti atoms during the spinodal decomposition.

It is interesting to note that according to SIFC-TDEP (symmetry-imposed force constants temperature-dependent effective potential method) modelling by Shulumba et al. [42], both the Al(Ti)N [ $(\text{Ti}_{0.12}\text{Al}_{0.88})\text{N}_{0.90}$ ] and the Ti(Al)N [ $(\text{Ti}_{0.30}\text{Al}_{0.70})_{0.97}\text{N}$ ] lamellae studied here have compositions not only in the metastable region, but also within the spinodal region. This means that there is a driving force for spinodal decomposition that of course requires sufficient time and temperature to occur. In addition, the spinodal region at 727 °C was calculated to cover the range  $0.27 < x < 0.97$  [for stoichiometric  $(\text{Ti}_{1-x}\text{Al}_x)\text{N}$ ]. The observed extremes in composition [the Al-richest of  $(\text{Ti}_{0.07}\text{Al}_{0.93})\text{N}_{0.64}$ , and the Ti-richest of  $(\text{Ti}_{0.72}\text{Al}_{0.28})_{0.88}\text{N}$ ] thus fit quite well with the predicted spinodal compositions at approximately the depositing temperature.

However, it is worth noting that due to the relatively low deposition temperature (around 650–750 °C [12,31]) used in the LPCVD process, decomposition during the CVD process is unlikely to happen. Such a process would also give more decomposition in the lower part of the coating than in the upper part, which is not observed. In addition, as has been reported in our previous work [12], the formation of a nanolamella structure in CVD TiAlN was linked to a rotational gas supply, instead of spinodal decomposition. It implies that bulk diffusion of Al and Ti should not happen during the formation of the nanolamella structure, but some surface diffusion could be possible at deposition temperature. Therefore, any fluctuations in chemistry, such as the variation of N non-stoichiometry and the varying Al and Ti contents, should be due to the deposition process itself, including surface adsorption, possibly surface diffusion of adsorbed species, surface reactions and possibly surface diffusion in the deposited layer before the next layer is formed.

Finally, it should be addressed that the N under- and over-stoichiometries found in the Al-rich and Ti-rich volumes in this work by APT are considered as vacancies in the N and metal sublattices, respectively, according to the DFT simulations of Baben et al. [20]. However, it is worth noting that the accuracy of the DFT simulations could be influenced by the limited supercell size and configurations of atoms.

## 5. Conclusions

In this work, we have studied 3D chemical content in LPCVD TiAlN coatings with a nanolamella structure using APT and complementary electron microscopy. Based on our findings we come to the following conclusions:

- The Ti(Al)N and the Al(Ti)N lamellae have over- and under-stoichiometries of N, respectively, due to a corresponding metal (Al and Ti) and N vacancy formation.

- In addition to the nanolamella structure, compositional variations on a scale of a few nm were found in both types of lamellae. The Ti-richest volumes have a maximum 12% of metal vacancies. The Al-richest volumes have a maximum 36% of N vacancies.
- The stoichiometric composition corresponds to  $(\text{Ti}_{0.18}\text{Al}_{0.82})\text{N}$ , which is close to the mean chemical composition.
- A small amount of Cl (around 0.1 at.%) exists in the coating, which implies incomplete dissociation of chloride precursors during the CVD surface reaction.

### Declaration of competing interest

None.

### Acknowledgements

Funding from “CVD 2.0”, a Swedish Foundation for Strategic Research program via SSF contract RMA15-0048 is gratefully acknowledged. This research was mainly carried out in the Chalmers Materials Analysis Laboratory (CMAL).

### Appendix A. Supplementary data

Supplementary data to this article can be found online at <https://doi.org/10.1016/j.surfcoat.2021.127741>.

### References

- J.M. Rodríguez, P. Jonsén, A. Svoboda, Simulation of metal cutting using the particle finite-element method and a physically based plasticity model, *Comput. Part. Mech.* 4 (2017) 35–51.
- T. Hoornaert, Z.K. Hua, J.H. Zhang, Hard wear-resistant coatings: a review, in: J. Luo, Y. Meng, T. Shao, Q. Zhao (Eds.), *Advanced Tribology*, Springer, Berlin Heidelberg, 2010.
- I. Endler, M. Höhn, M. Herrmann, R. Pitonak, S. Ruppi, M. Schneider, H. van den Berg, H. Westphal, Novel aluminum-rich  $\text{Ti}_{1-x}\text{Al}_x\text{N}$  coatings by LPCVD, *Surf. Coat. Technol.* 203 (2008) 530–533.
- J. Todt, J. Zalesak, R. Daniel, R. Pitonak, A. Köpf, R. Weißenbacher, B. Sartory, C. Mitterer, J. Keckes, Al-rich cubic  $\text{Al}_{0.8}\text{Ti}_{0.2}\text{N}$  coating with self-organized nanolamellar microstructure: thermal and mechanical properties, *Surf. Coat. Technol.* 291 (2016) 89–93.
- S. PalDey, S.C. Deevi, Single layer and multilayer wear resistant coatings of (Ti,Al) N: a review, *Mater. Sci. Eng. A* 342 (2003) 58–79.
- R. Qiu, A. Forslund, O. Bäcke, A.H.S. Iyer, M. Sattari, W. Janssen, T. Manns, J. Kümmel, A. Ruban, D. Stiens, H.-O. André, M. Halvarsson, Effects of gas flow on detailed microstructure inhomogeneities in LPCVD TiAlN nanolamella coatings, *Materialia* 9 (2020), 100546.
- A. Kimura, H. Hasegawa, K. Yamada, T. Suzuki, Metastable  $\text{Ti}_{1-x}\text{Al}_x\text{N}$  films with different Al content, *J. Mater. Sci. Lett.* 19 (2000) 601–602.
- M. Zhou, Y. Makino, M. Nose, K. Nogi, Phase transition and properties of Ti–Al–N thin films prepared by r.f.-plasma assisted magnetron sputtering, *Thin Solid Films* 339 (1999) 203–208.
- U. Wahlström, L. Hultman, J.E. Sundgren, F. Adibi, I. Petrov, J.E. Greene, Crystal growth and microstructure of polycrystalline  $\text{Ti}_{1-x}\text{Al}_x\text{N}$  alloy films deposited by ultra-high-vacuum dual-target magnetron sputtering, *Thin Solid Films* 235 (1993) 62–70.
- M. Meindlumer, J. Zalesak, R. Pitonak, J. Todt, B. Sartory, M. Burghammer, A. Stark, N. Schell, R. Daniel, J.F. Keckes, M. Lessiak, A. Köpf, R. Weißenbacher, J. Keckes, Biomimetic hard and tough nanoceramic Ti–Al–N film with self-assembled six-level hierarchy, *Nanoscale* 11 (2019) 7986–7995.
- J. Zalesak, D. Holec, I. Matko, M. Petreenc, B. Sartory, N. Koutná, R. Daniel, R. Pitonak, J. Keckes, Peculiarity of self-assembled cubic nanolamellae in the TiN/AlN system: epitaxial self-stabilization by element deficiency/excess, *Acta Mater.* 131 (2017) 391–399.
- R. Qiu, O. Bäcke, D. Stiens, W. Janssen, J. Kümmel, T. Manns, H.-O. André, M. Halvarsson, CVD TiAlN coatings with tunable nanolamella architectures, *Surf. Coat. Technol.* 413 (2021), 127076.
- M. Ben Hassine, H.-O. André, A.H.S. Iyer, A. Lotsari, O. Bäcke, D. Stiens, W. Janssen, T. Manns, J. Kümmel, M. Halvarsson, Growth model for high-Al containing CVD TiAlN coatings on cemented carbides using intermediate layers of TiN, *Surf. Coat. Technol.* 421 (2021), 127361.
- C.-S. Shin, D. Gall, N. Hellgren, J. Patscheider, I. Petrov, J.E. Greene, Vacancy hardening in single-crystal  $\text{TiN}_x(001)$  layers, *J. Appl. Phys.* 93 (2003) 6025–6028.
- I.C. Schramm, M.P. Johansson Jöesaar, J. Jensen, F. Mücklich, M. Odén, Impact of nitrogen vacancies on the high temperature behavior of  $(\text{Ti}_{1-x}\text{Al}_x)\text{N}_y$  alloys, *Acta Mater.* 119 (2016) 218–228.
- S.-H. Jhi, S.G. Louie, M.L. Cohen, J. Ihm, Vacancy hardening and softening in transition metal carbides and nitrides, *Phys. Rev. Lett.* 86 (2001) 3348–3351.
- I.A. Abrikosov, A. Knutsson, B. Alling, F. Tasnádi, H. Lind, L. Hultman, M. Odén, Phase stability and elasticity of TiAlN, *Materials* 4 (2011).
- M. to Baben, M. Hans, D. Primetzhofer, S. Evertz, H. Ruess, J.M. Schneider, Unprecedented thermal stability of inherently metastable titanium aluminum nitride by point defect engineering, *Mater. Res. Lett.* 5 (2017) 158–169.
- R. Qiu, Electron Microscopy Investigation of Detailed Microstructures of CVD TiAlN and TiN Coatings - Effects of Gas Flow and Substrate on Coating Microstructure, Licentiate thesis, Chalmers University of Technology, 2020.
- M. to Baben, L. Raumann, D. Music, J.M. Schneider, Origin of the nitrogen over- and understoichiometry in  $\text{Ti}_{0.5}\text{Al}_{0.5}\text{N}$  thin films, *J. Phys. Condens. Matter.* 24 (2012), 155401.
- H. Euchner, P.H. Mayrhofer, Vacancy-dependent stability of cubic and wurtzite  $\text{Ti}_{1-x}\text{Al}_x\text{N}$ , *Surf. Coat. Technol.* 275 (2015) 214–218.
- A. Paseuth, K. Yamagata, A. Miura, M. Higuchi, K. Tadanaga, M. Cinibulk, Deposition and analysis of Al-rich c-Al<sub>0.5</sub>Ti<sub>0.5</sub>N coating with preferred orientation, *J. Am. Ceram. Soc.* 100 (2016) 343–353.
- B. Gault, A.J. Breen, Y. Chang, J. He, E.A. Jäggle, P. Kontis, P. Kürmsteiner, A. Kwiatkowski da Silva, S.K. Mäkinen, I. Mouton, Z. Peng, D. Ponge, T. Schwarz, L. T. Stephenson, A. Szczepaniak, H. Zhao, D. Raabe, Interfaces and defect composition at the near-atomic scale through atom probe tomography investigations, *J. Mater. Res.* 33 (2018) 4018–4030.
- R. Rachbauer, E. Stergar, S. Massl, M. Moser, P.H. Mayrhofer, Three-dimensional atom probe investigations of Ti–Al–N thin films, *Scr. Mater.* 61 (2009) 725–728.
- R. Rachbauer, S. Massl, E. Stergar, P. Felfel, P.H. Mayrhofer, Atom probe specimen preparation and 3D interfacial study of Ti–Al–N thin films, *Surf. Coat. Technol.* 204 (2010) 1811–1816.
- L.J.S. Johnson, M. Thuvander, K. Stiller, M. Odén, L. Hultman, Spinodal decomposition of  $\text{Ti}_{0.33}\text{Al}_{0.67}\text{N}$  thin films studied by atom probe tomography, *Thin Solid Films* 520 (2012) 4362–4368.
- I.C. Schramm, C. Pauly, M.P. Johansson Jöesaar, S. Slawik, S. Suarez, F. Mücklich, M. Odén, Effects of nitrogen vacancies on phase stability and mechanical properties of arc deposited  $(\text{Ti}_{0.52}\text{Al}_{0.48})\text{N}_y$  ( $y < 1$ ) coatings, *Surf. Coat. Technol.* 330 (2017) 77–86.
- T. Lehmann, High resolution analysis of  $\text{Ti}_x\text{Al}_{1-x}\text{N}$  hard coatings, Master Thesis, University of Stuttgart, 2018.
- M. Hans, J.M. Schneider, On the chemical composition of TiAlN thin films — comparison of ion beam analysis and laser-assisted atom probe tomography with varying laser pulse energy, *Thin Solid Films* 688 (2019), 137251.
- M. Hans, J.M. Schneider, Electric field strength-dependent accuracy of TiAlN thin film composition measurements by laser-assisted atom probe tomography, *New J. Phys.* 22 (2020) 33036.
- D. Stiens, T. Manns, S. Ruppi, TiAlCN layers with lamellae structure, US patent 10,214,810 B2, 2019.
- R.R. Cerchiara, P.E. Fischione, J. Liu, J.M. Matesa, A.C. Robins, H.L. Fraser, A. Genc, Raising the standard of specimen preparation for aberration-corrected TEM and STEM, *Microsc. Today* 19 (2011) 16–19.
- D. Shinde, L. Arnoldi, A. Devaraj, A. Vella, Laser-material interaction during atom probe tomography of oxides with embedded metal nanoparticles, *J. Appl. Phys.* 120 (2016), 164308.
- L. Arnoldi, A. Vella, J. Houard, B. Deconihout, Antenna effect in laser assisted atom probe tomography: how the field emitter aspect ratio can enhance atomic scale imaging, *Appl. Phys. Lett.* 101 (2012), 153101.
- J. Angseryd, F. Liu, H.-O. André, S.S.A. Gerstl, M. Thuvander, Quantitative APT analysis of Ti(C,N), *Ultramicroscopy.* 111 (2011) 609–614.
- A. Forslund, A. Ruban, Surface energetics of  $\text{Al}_x\text{Ti}_{1-x}\text{N}$  alloys, *Comput. Mater. Sci.* 183 (2020), 109813.
- B. Gault, D.W. Saxe, M.W. Ashton, S.B. Sinnott, A.N. Chiamonti, M.P. Moody, D. K. Schreiber, Behavior of molecules and molecular ions near a field emitter, *New J. Phys.* 18 (2016) 33031.
- E. Di Russo, I. Blum, J. Houard, M. Gilbert, G. Da Costa, D. Blavette, L. Rigutti, Compositional accuracy of atom probe tomography measurements in GaN: impact of experimental parameters and multiple evaporation events, *Ultramicroscopy* 187 (2018) 126–134.
- R.J.H. Morris, R. Cuduvally, D. Melkonyan, C. Fleischmann, M. Zhao, L. Arnoldi, P. van der Heide, W. Vandervorst, Toward accurate composition analysis of GaN and AlGaIn using atom probe tomography, *J. Vac. Sci. Technol. B* 36 (2018), 03F130.
- K. Yalamanchili, F. Wang, H. Aboulfadl, J. Barrirero, L. Rogström, E. Jiménez-Pique, F. Mücklich, F. Tasnadi, M. Odén, N. Ghafoor, Growth and thermal stability of TiN/ZrAlN: effect of internal interfaces, *Acta Mater.* 121 (2016) 396–406.
- B. Gault, M.P. Moody, J.M. Cairney, S.P. Ringer, *Atom Probe Microscopy*, Springer, New York, NY, 2012.
- N. Shulumba, O. Hellman, Z. Raza, B. Alling, J. Barrirero, F. Mücklich, I. A. Abrikosov, M. Odén, Lattice vibrations change the solid solubility of an alloy at high temperatures, *Phys. Rev. Lett.* 117 (2016), 205502.